Title

An Intravascular Tantalum Oxide-based CT Contrast Agent: Preclinical Evaluation Emulating Overweight and Obese Patient Size.

Journal

Radiology, 289(1)

ISSN

0033-8419

Authors

Lambert, Jack W
Sun, Yuxin
Stillson, Carol
et al.

Publication Date

2018-10-01

DOI

10.1148/radiol.2018172381

Peer reviewed

An Intravascular Tantalum Oxide–based CT Contrast Agent: Preclinical Evaluation Emulating Overweight and Obese Patient Size

Jack W. Lambert, PhD • Yuxin Sun, MS • Carol Stillson, RVT • Zhixi Li, MD • Rahi Kumar, MD • Sizhe Wang, MS • Paul F. FitzGerald, AAS • Peter J. Bonitatibus, Jr, PhD • Robert E. Colborn, PhD • Jeannette C. Roberts, MS • Peter M. Edic, PhD • Michael Marino, PhD • Benjamin M. Yeh, MD

From the Department of Radiology and Biomedical Imaging, University of California San Francisco, 505 Parnassus Ave, San Francisco, CA 94143-0628 (J.W.L., Y.S., C.S., Z.L., R.K., S.W., B.M.Y.); and Departments of Imaging (P.F.F., P.M.E.) and Biosciences (P.J.B., R.E.C., J.C.R., M.M.), GE Global Research, Niskayuna, NY. Received October 13, 2017; revision requested November 14; revision received March 28, 2018; accepted March 30. **Address correspondence to** B.Y. (e-mail: *Ben.Yeh@ucsf.edu*).

Supported by the National Institute of Biomedical Imaging and Bioengineering (R01EB015476).

Conflicts of interest are listed at the end of this article.

Radiology 2018; 289:103–110 • https://doi.org/10.1148/radiol.2018172381 • Content code: GI

Purpose: To compare the CT imaging performance of a carboxybetaine zwitterionic–coated tantalum oxide (TaCZ) nanoparticle CT contrast agent with that of a conventional iodinated contrast agent in a swine model meant to simulate overweight and obese patients.

Materials and Methods: Four swine were evaluated inside three different-sized adipose-equivalent encasements emulating abdominal girths of 102, 119, and 137 cm. Imaging was performed with a 64–detector row CT scanner at six scan delays after intravenous injection of 240 mg element (Ta or I) per kilogram of body weight of TaCZ or iopromide. For each time point, contrast enhancement of the aorta and liver were measured by using regions of interest. Two readers independently recorded the clarity of vasculature using a five-point Likert scale. Findings were compared by using paired *t* tests and Wilcoxon signed-rank tests.

Results: Mean peak enhancement was higher for TaCZ than for iopromide in the aorta (270 HU [σ = 24.5] vs 199 HU [σ = 10.2], $P < .001$) and liver (61.3 HU [σ = 11.7] vs 45.2 HU [σ = 8], $P < .001$). Vascular clarity was higher for TaCZ than for iopromide in 63% (132 of 208), 82% (170 of 208), and 86% (178 of 208) of the individual vessels at the 102-, 119-, and 137-cm girths, respectively ($P < .01$). Arterial clarity scores were higher for TaCZ than for iopromide in 62% (208 of 336) of vessels. Venous clarity scores were higher for TaCZ than for iopromide in 89% (128 of 144) of the veins in the venous phase and in 100% (144 of 144) of veins in the delayed phase ($P < .01$). No vessel showed higher clarity score with iopromide than with TaCZ.

Conclusion: An experimental tantalum nanoparticle–based contrast agent showed greater contrast enhancement compared with iopromide in swine models meant to simulate overweight and obese patients.

Intravascular contrast agents provide vital diagnostic information for CT imaging; therefore, they are used in approximately half of the 85 million CT scans performed annually in the United States (1). Iodine is used as the reporter element in all current intravascular CT contrast materials. No substantively new CT contrast agent has been approved for clinical use in over 2 decades (1). Although iodine provides adequate contrast enhancement at the low x-ray tube potentials required for imaging small patients, the intensity of enhancement from iodinated contrast agents decreases by up to 50% at the high x-ray tube potentials required for imaging overweight and obese patients (2). Consequently, iodine-enhanced CT image quality is particularly poor for imaging the abdomen in overweight and obese patients. The poor performance of iodinated contrast agents in overweight and obese patients is a key limitation for patient care in this high-risk population for whom imaging is particularly important due to myriad obesity-related comorbidities (3).

There is reduced contrast enhancement of iodine with high tube potential because iodine has a k-edge energy of 33 keV. Above this threshold, x-ray attenuation decreases monotonically. The mean photon energies of 80-, 100-, 120-, and 140-kVp x-ray spectra are approximately 60, 68, 81, and 93 keV, respectively (2); thus, as tube potential is increased, the mean photon energy is further from the iodine k-edge, and the attenuation provided by iodine is reduced accordingly. At the high-tube-potential settings required to penetrate overweight patients, poor iodine contrast enhancement can severely impede diagnostic utility (2,4,5). This problem is compounded by hardening of the x-ray spectrum, which is a function of path length and is more severe in overweight and obese patients (6).

High-atomic-number elements, such as ytterbium ($Z = 70$), hafnium ($Z = 72$), tantalum ($Z = 73$), tungsten ($Z = 74$), gold ($Z = 79$), and bismuth ($Z = 83$), have been proposed as alternative reporter elements, as their high k-edges attenuate more x-rays in the diagnostic energy range (7–19). Among the candidate elements with a high atomic number, screening studies have identified nanoparticles of tantalum (k-edge = 67.4 keV) as a cost-effective and biocompatible option capable of providing superior contrast levels over a wide range of patient sizes (2,20). An intravascular carboxybetaine zwitterionic

Abbreviations

ROI = region of interest, TaCZ = carboxybetaine zwitterionic tantalum oxide

Summary

An experimental tantalum oxide nanoparticle–based contrast agent provided improved vascular enhancement compared with a conventional iodinated agent in swine models meant to simulate overweight and obese patients.

Implications for Patient Care

- The use of a tantalum-based contrast agent has potential to improve CT vascular image quality in overweight and obese patients and thereby increase diagnostic confidence in this high-risk population.
- The superior contrast enhancement offered by tantalum could also enable use of lower injected contrast agent doses, radiation doses, or both because of the greater contrast-to-noise ratio of the tantalum-based contrast agent compared with that of iodine-based contrast agents.

tantalum oxide (TaCZ) nanoparticle agent has recently been described as showing promising physicochemical and biologic properties (12). In a pilot experiment using a rat model placed in the mediastinal insert of a thorax phantom that simulated the size of an overweight adult patient, TaCZ was shown to offer improved enhancement when compared with iopromide (12). No adverse effects were seen, and organ retention was similar to that of existing commercial iodine agents in rats (12). However, as with all other preclinical studies of high-atomic-number contrast agents (7,8,10,11,21), the small-animal model precluded anatomically relevant image quality analysis. As such, these key properties remained untested in large-animal models for all high-atomic-number contrast agent candidates.

The purpose of this study was to compare the CT imaging performance of TaCZ with that of iopromide in a porcine model encased within attenuators to simulate overweight and obese patients. We sought a comprehensive comparison using multiple simulated patient diameters, multiple scans per diameter, and multiple time points per scan; for evaluation, we used both objective and subjective image quality metrics.

Materials and Methods

Encasements

Three custom-made adipose-equivalent plastic encasements (Computerized Imaging Reference Systems, Norfolk, Va) 30 cm in length were used to increase abdominal girth of the porcine model (Table 1). Swine abdomens were scanned in the supine position and were centrally placed within the encasements, with polyethylene bladders containing canola oil used to fill in the air gaps with adipose-equivalent material (Fig 1). In addition to providing an additional cross-sectional area to emulate overweight and obese patients, these encasements provided consistent outer girths and shape to enable direct comparison between studies, independent of the encased pigs' abdomen sizes, by using equal radiation dose and thereby obtaining equivalent image noise for all scans with each encasement size.

Animals

Care and maintenance of experimental animals was in accordance with National Institutes of Health guidelines and with the rules of our committee on animal research. Four female Yorkshire domestic swine (Pork Power Farms, Turlock, Calif) with a mean weight of 51 kg (range, 29–68 kg) on the day of scanning underwent 12 separate scanning sessions. Individual swine were housed at our institution and grew over a period of several weeks to 3 months. Prior to each scanning session, animals were fasted from the prior afternoon. On the day of scanning, animals were sedated with intramuscular injection of tiletamine hydrochloride and zolazepam hydrochloride (2.0 mg per kilogram of body weight, Telazol; Zoetis, Kalamazoo, Mich). Endotracheal intubation was performed in the standard fashion, and anesthesia was maintained with isoflurane (Attane; Piramal Critical Care, Bethlehem, Pa) at 1%–5% to effect with oxygen at 2.0 L/min. An auricular vein catheter was placed for contrast material administration, and atropine sulfate (0.04 mg/kg; Abbott Laboratories, North Chicago, Ill) was given intravenously to reduce oral secretions. Ventilation was provided with a volume-controlled ventilator (2002 Pro; Hallowell Engineering & Manufacturing Corporation, Pittsfield, Mass), and anesthesia was maintained with isoflurane. Animals were monitored with electrocardiography, end-tidal carbon dioxide monitoring, and pulse oximetery at all times. TaCZ, formulated as previously described (12), and iopromide (300 mg of iodine per milliliter, Ultravist; Bayer Healthcare, Wayne NJ) were diluted to a mass concentration of 240 mg active element per milliliter, and one of the two was injected via a CT power injector (Medrad Stellant, Bayer Healthcare) at a constant rate for a 30-second injection of 540 mg of the active element per kilogram of body weight. This was followed by a 10-second saline injection at the same rate. After scanning, buprenorphine hydrochloride (0.01 mg/kg, Buprenex; Hospira, Lake Forest, Ill) was administered intramuscularly as an analgesic, and cefazolin (22 mg/kg, Ancef; West-Ward Pharmaceuticals, Eatontown, NJ) was administered intravenously. After imaging, animals were weaned off the ventilator and recovered. The following week, animals were scanned in the same adipose-equivalent encasement, and the other contrast agent was injected to enable same-animal comparisons of the two contrast materials. The order of iopromide and TaCZ was randomized, such that half the swine received each agent first.

Imaging

A 64–detector row CT scanner (Discovery CT750 HD; GE Healthcare, Chicago, Ill) was used in the helical mode (0.984:1 pitch, 40-mm collimation, 0.5-second gantry rotation time, large-body bowtie filter, fixed tube current dependent on the adipose-equivalent encasement size) (Table 1). Scan lengths of 30 cm (the z-axis length of the adipose-equivalent encasements) were used, resulting in a 4.4-second scan. The adipose-equivalent encasements were aligned cranially to include the dome of the swine liver in each scan, and the canola oil bags were placed between the swine and the encasement. CT tech-

Table 1: Adipose-equivalent Plastic Encasement Sizes and Corresponding CT Protocols for the Three Simulated Patient Sizes

Encasement Girth	Inner Diameter (cm)		Outer Diameter (cm)		Plastic Encasement Thickness (cm)	Tube Potential (kVp)	Tube Current (mA)	$CTDI_{vol}$ (mGy)	SSDE (mGy)
	AP	LAT	AP	LAT					
102 cm	25.0	32.5	28.5	36.5	3.25	100	595	14.6	15.6
119 cm	28.5	36.5	34.0	42.0	2.75	120	675	26.4	22.7
137 cm	28.5	36.5	40.0	48.0	5.75	140	575	32.0	23.0

Note.—AP = anterposterior, LAT = transverse, $CTDI_{vol}$ = volume CT dose index, SSDE = size-specific dose estimate.

niques were designed to produce similar image noise between the three encasement sizes at clinically relevant x-ray tube potentials and radiation doses (Table 1). Scans were performed during an end-expiration breath hold immediately prior to injection and at scan delays of 29, 39, 60, 80, 180, and 300 seconds after the start of injection. These scan delay time points were informed by a prior investigation into intravascular contrast dynamics of swine (22) and were chosen to produce two each of arterial, portal venous, and delayed phase data sets. Axial images were reconstructed with a 50-cm field of view and a 2.5-mm section thickness and spacing by using filtered back projection and a standard kernel.

Objective Image Quality Assessment

One reader with 3 years of experience with small- and large-animal imaging for contrast material development and an MS degree in biomedical imaging (Y.S.) placed regions of interest (ROIs) in homogeneous regions of the abdominal aorta and the liver parenchyma to measure CT numbers before contrast material administration and at the six delayed time points after contrast material administration among the 12 data sets (two contrast agents × three encasement sizes × two repetitions). In the liver, care was taken to avoid visible hepatic vasculature. Consequently, ROI size and shape varied but included at least five axial image ROIs with a total area of at least 500 mm^2 at each time point and organ. Within each data set, unenhanced results were subtracted from contrast material–enhanced results to determine net contrast enhancement. Image noise was recorded as the standard deviation of CT number (in Hounsfield units) in ROIs placed in the canola oil bags. The percentage reduction from peak enhancement to enhancement during the final imaging time point was calculated.

Subjective Image Quality Assessment

Two radiologists with abdominal imaging subspecialty training (R.K., Z.L.; 5 and 4 years of experience reading abdominal CT images, respectively) viewed images from the six contrast-enhanced time points in each of the 12 data sets. The order of the images was randomized and the readers were not aware of the type of contrast material used for each scan. Images were viewed by using a standard clinical picture archiving and communication system (Impax ES, version 6; Agfa Technical Imaging Systems, Ridgefield Park, NJ) with default soft-tissue window settings (window width, 400 HU; window level, 40 HU); however, readers were free to change settings to suit preferences. For each scan, the readers graded the subjective image noise and severity of image artifacts on five-point Likert scales. The subjective image noise was graded as follows: 0, unacceptably high; 1, higher than average; 2, average; 3, lower than average; and 4, minimal. The severity of image artifacts was graded as follows: 0, major, preventing diagnosis; 1, pronounced, interfering with diagnosis; 2, moderate; 3, mild, not interfering with diagnosis; and 4, absent. At each of the six time points for each scan, the overall vascular image quality was graded as follows: 0, nondiagnostic; 1, limited; 2, adequate; 3, good; and 4, excellent. Seven specific arteries (the aorta and the celiac, common hepatic, gastroduodenal, branch hepatic, epigastric and splenic arteries) were graded at the first four time points (29, 39, 60, and 80 seconds) by using the following scale: 0, not seen; 1, faintly seen or visible but discontinuous; 2, continuous but neither origin nor branch are well seen; 3, continuous but either origin or branch not well seen; and 4, clearly defined with origin and branches seen. Six specific veins (the infrahepatic inferior vena cava and the portal, right hepatic, midhepatic, left hepatic, and splenic veins) were graded at the later four time points (60, 80, 180, and 300 seconds) by using the same scale. These data were divided into portal venous phases (60 and 80 seconds) and delayed phases (180 and 300

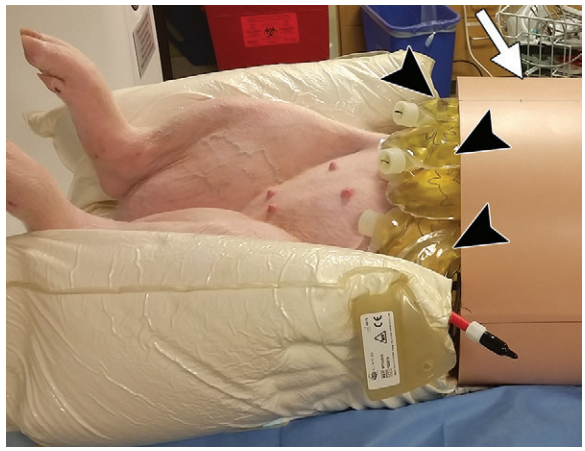

Figure 1: Supine swine on CT scanner table. Anesthetized swine is within an adipose-equivalent plastic encasement (arrow) that measures 30 cm in the z-axis. Polyethylene bladders containing canola oil (arrowheads) were used to fill the air gaps between the swine abdomen and the adipose-equivalent plastic encasement.

seconds). Since individual swine were imaged with each contrast agent on different days, this approach yielded 57 matched vessel pairs for comparison (three encasement sizes, seven arteries, six veins in the venous phases, six veins in the delayed phases). Mean scores among the two readers were compared for the two contrast agents. Data were also grouped by vessel type and simulated patient size to assess trends.

Statistical Analyses

All statistical analyses were performed by using Excel software (2011 version; Microsoft, Redmond, Wash). ROI measurements of image noise, aorta enhancement, and liver enhancement were assessed by using paired *t* tests. Qualitative vascular scores between the two contrast agents were assessed by using the Wilcoxon signed rank test. Interobserver agreement was assessed by using a weighted k test. For all analyses, statistical significance was defined as $P < .05$ in two-tailed hypothesis tests.

Results

Objective Image Quality Assessment

No difference in image noise was observed between iopromide and TaCZ scans at any of the simulated patient sizes ($P > .5$) (Table 2). At all simulated patient sizes, peak enhancement of the aorta and liver was significantly higher for TaCZ than for iopromide ($P < .005$) (Table 2). At the 102-cm girth, peak aortic enhancement occurred at 39 seconds for both contrast agents, while for the 119- and 137-cm girths it occurred at 29 seconds (Fig 2a). Peak hepatic enhancement occurred at 60 seconds for both contrast agents in all simulated patient sizes (Fig 2b). After peak enhancement, TaCZ continued to display significantly higher contrast material retention in both the aorta and the liver (Fig 2a, 2b).

Subjective Image Quality Assessment

Interobserver agreement was moderate, with a weighted κ value of 0.60 (23). Subjective image noise and artifacts were not significantly different between scans with the two contrast agents (Fig 3). Overall vascular image quality was higher for TaCZ than for iopromide at all three encasement sizes, with TaCZ graded higher than iopromide in 75% (18 of 24), 88% (21 of 24), and 96% (23 of 24) of the data sets for the 102-, 119-, and 137-cm girths, respectively ($P < .01$) (Fig 3). Conversely, vascular image quality was not graded higher for iopromide than for TaCZ in any of the grading pairs. Among the 57 individual vessel grading pairs, TaCZ was scored higher than iopromide in 54 instances ($P < .05$), with no significant difference observed between the three pairs. The three pairs were the aorta, epigastric artery, and splenic vein, all at the 102-cm girth. When grouping the data by vessel type, TaCZ was graded higher than iopromide in 62% (208 of 336) of the arteries (graded at 29–80 seconds) (Fig 4a), 89% (128 of 144) of the veins in the venous phase (60–80 seconds) (Fig 4b), and 100% (144 of 144) of the veins in the delayed phase (180, 300 seconds) (Fig 4c). When grouping the data by simulated patient size, TaCZ was graded higher than iopromide in 63% (132 of 208), 82% (170 of 208), and 86% (178 of 208) of ves-

Table 2: Background Image Noise and Net Peak Aortic and Hepatic CT Number Enhancement for the Two Contrast Agents

Encasement Girth	Image Noise (HU)			Peak Aortic Enhancement (HU)			Peak Hepatic Enhancement (HU)		
	Iopromide	Tantalum Oxide	Increase for Tantalum Oxide Compared with Iopromide (%)	Iopromide	Tantalum Oxide	Increase for Tantalum Oxide Compared with Iopromide (%)	Iopromide	Tantalum Oxide	Increase for Tantalum Oxide Compared with Iopromide (%)
102 cm	17.6 ± 1.5	17.5 ± 1.4	−0.6	244 ± 12	291 ± 22	19*	56.2 ± 8.8	70.7 ± 8.7	26*
119 cm	17.0 ± 1.1	17.0 ± 1.2	0	198 ± 11	289 ± 34	46*	43.4 ± 8.4	60.2 ± 13	39*
137 cm	20.2 ± 1.3	20.2 ± 1.3	0	154 ± 8.4	229 ± 17	49*	36.0 ± 6.7	53.0 ± 13	47*

Note.—Unless otherwise indicated, data are mean ± standard deviation among the region-of-interest measurements for the two scans per condition.
* Denotes a significant difference between the two contrast agents, as determined with a paired *t* test ($P < .05$).

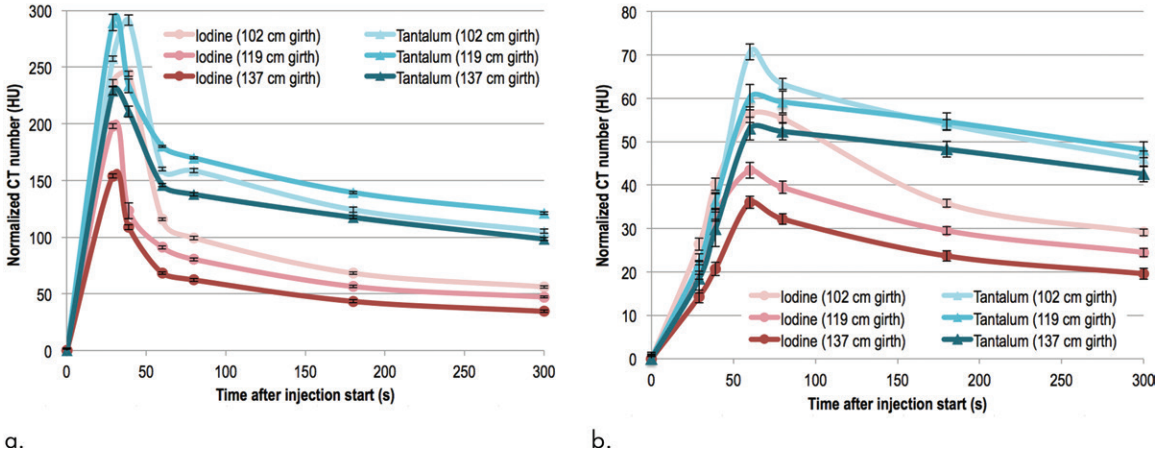

Figure 2: Graphs show mean contrast enhancement for iopromide and tantalum oxide for the three simulated patient girths in the **(a)** abdominal aorta and **(b)** liver parenchyma. Error bars represent standard errors among the 12–24 region-of-interest measurements per data point.

sels for the 102-, 119-, and 137-cm girths, respectively. Conversely, iopromide was not graded higher than TaCZ in any of the individual vessel grading pairs. Portal venous phase images of the two contrast agents at the level of the liver showed superior vascular and liver contrast enhancement from TaCZ at all encasement sizes (Fig 5).

Discussion

Our study explored the potential value of high-atomic-number elements for CT imaging of overweight and obese body habitus by using a large-animal model. We found that TaCZ provides superior vascular and hepatic enhancement in vivo in a swine model meant to simulate overweight or obese patients (range, 102–137-cm abdominal girth) when compared with the same mass dose of an iodinated small-molecule contrast agent (iopromide) imaged with identical scanning parameters. Since the atomic mass of tantalum is 43% greater than that of iodine (181 vs 127), the molar dose of iodine was 43% larger than that of tantalum.

We found that TaCZ provided higher peak enhancement than did iopromide in both the aorta and the liver. Also, TaCZ-enhanced scans yielded higher qualitative vessel image quality scores than did iopromide-enhanced scans in the abdominal arteries and veins at all simulated patient sizes. The higher contrast enhancement for TaCZ-enhanced scans was likely due to the higher k-edge energy of tantalum compared with that of iodine. The enhancement increases for TaCZ-enhanced scans compared with iopromide-enhanced scans were 19%, 46%, and 48% at 100, 120, and 140 kVp, respectively, in the aorta and 26%, 39%, and 47% at the same tube potentials in the liver; these correlated reasonably well with previously reported results in phantoms, which showed enhancement increases of 24%, 46%, and 60% for tantalum compared with iodine at 100 kVp, 120 kVp, and 140 kVp, respectively (2).

A relatively low operating voltage of 100 kVp has been proposed as a more dose-efficient alternative to the conventional 120-kVp setting for iodine-enhanced scanning of adult abdomens, as the increased iodine enhancement yields

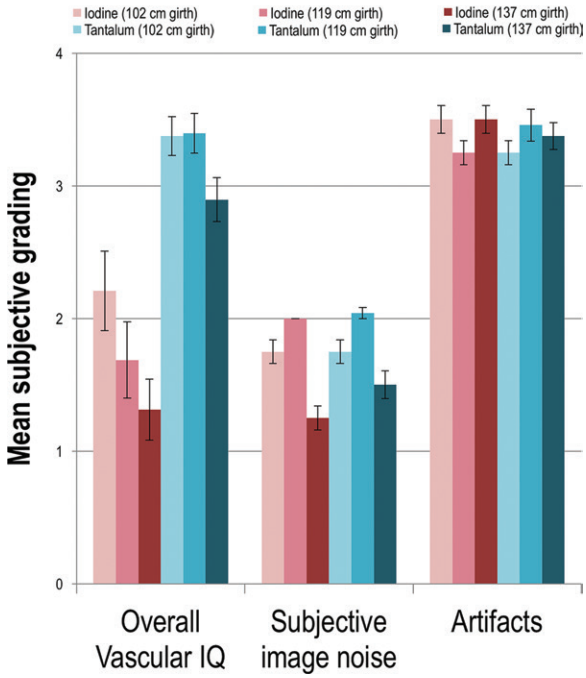

Figure 3: Mean general image quality scores for iopromide and tantalum oxide at the three simulated patient sizes. Differences between contrast agents in overall vascular image quality were significant at all three sizes ($P < .01$). Error bars represent standard errors among the 24 reader scores per data point. IQ = image quality.

a higher contrast-to-noise ratio, and thus greater dose efficiency, at an equal dose (24–26). Thus, to provide optimal imaging conditions for iodine, we chose 100 kVp for imaging the 102-cm encasement size in our study. The significantly better performance of TaCZ over that of iopromide that was observed when scanning under these conditions suggests that the benefits of the TaCZ agent might be observed in a large majority of adult patient sizes, with the likely exception of those that can be successfully scanned with a lower tube potential, such as 80 or 70 kVp.

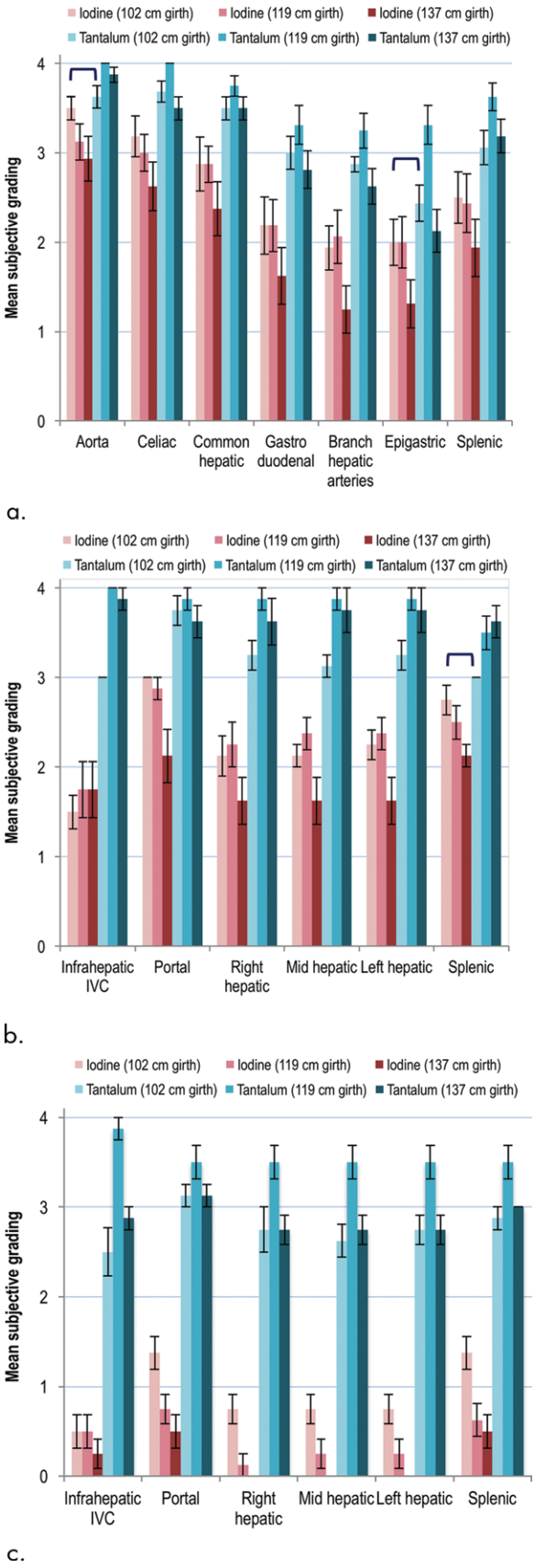

Figure 4: Bar graphs show individual vessel image quality scores for the two readers for iopromide and tantalum oxide at the three simulated patient sizes. **(a)** Mean artery scores from 29-, 39-, 60-, and 80-second time points. **(b)** Mean vein scores from 60- and 80-second portal venous phase time points. **(c)** Mean vein scores from 180- and 300-second delayed-phase time points. Brackets over matched pairs indicate differences that were not significant ($P > .05$). Error bars represent the standard error among the eight to 16 individual scores per data point.

We also observed sustained contrast enhancement shown by TaCZ over the 5-minute scanning period. Whereas iopromide exhibited a peak-to-300-second contrast reduction of 77.1% in the aorta, only a 59.4% reduction was seen for TaCZ. This corresponded to pronounced improvements in subjective venous image quality scores at the later time points. Similar to findings in aortic enhancement, the decline in peak-to-300-second enhancement was lower with TaCZ than with iopromide. However, the overall clearance rate of TaCZ was previously shown to be similar to those of iodine-based agents (12). This sustained enhancement during the typical scan delays used for clinical imaging suggests that TaCZ may have promising implications for liver imaging, where excellent enhancement during multiphasic contrast-enhanced examinations, including the delayed phase, are critical to tumor detection, characterization, and presurgical planning (27,28).

Our study had several limitations. First, a concentration of 240 mg element per milliliter was used for both agents, representing the lower end of the range used in clinical practice. This was required to accommodate the osmolality and viscosity properties of TaCZ, which is still in development (12). For both agents, the same contrast agent volume (2.25 mL/kg) and the same mass dose of tantalum as for iodine (540 mg element/kg) was delivered. We are currently optimizing TaCZ to enable administration at higher concentrations. Despite this limitation, it is unlikely that the maximum concentration of iopromide (370 mg/mL) would offset the dramatic enhancement reduction that occurs in overweight and obese patient sizes, particularly at venous and delayed scan phases. Second, although we assessed vascular image quality in healthy animals, we did not image animals with disease, and the sample size is small. Our promising data justify future in vivo studies to assess the ability of TaCZ to improve contrast enhancement and lesion detection and characterization. Third, it is likely that the tantalum oxide nanoparticle agent, which is physically larger than the iopromide molecule, has a slower rate and extent of distribution into the extravascular extracellular space than does iopromide, which is known to quickly equilibrate between intravascular and interstitial fluid. A higher intravascular concentration of tantalum oxide may contribute to the improved vascular delineation seen with the tantalum oxide agent compared with that seen with iopromide, particularly at longer scan delays (non–arterial-phase scans). Fourth, we only investigated imaging performance in models meant to simulate overweight and obese patients. Nevertheless, these represent approximately half of the population in the United States (29), and obese patients are a particularly challenging population, for whom satisfactory abdominal CT image quality is currently unobtainable and in whom disease prevalence is high. Fifth, our study evaluated a single set of injection protocols and scan delays in healthy swine. Future exploration of doses and injection protocols will be

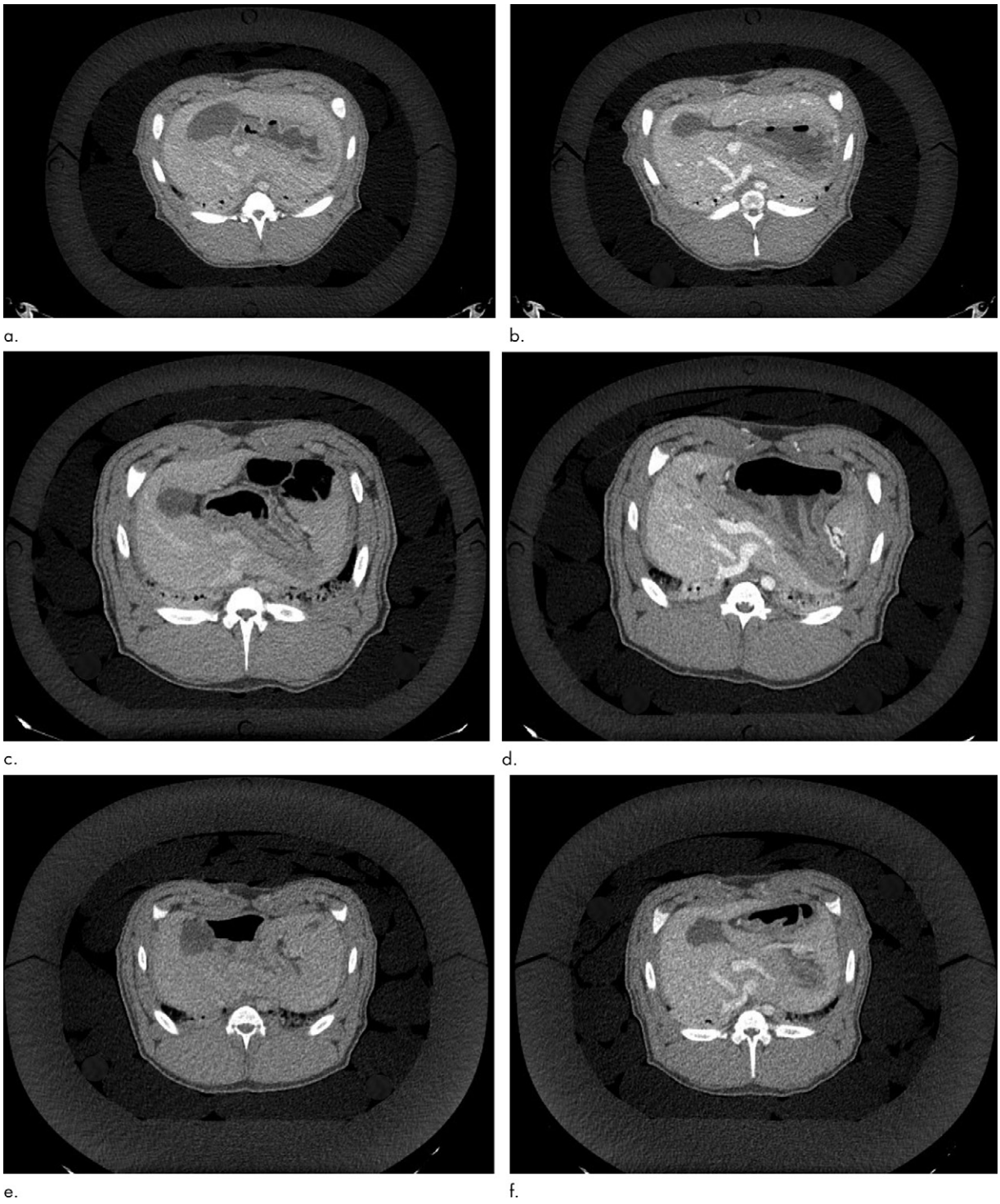

Figure 5: Axial CT images in the porcine model within three different-sized adipose-equivalent encasements show iopromide (left) and tantalum oxide (right) contrast agents at the level of the liver 80 seconds after the start of injection at simulated patient girths of **(a, b)** 102, **(c, d)** 119, and **(e, f)** 137 cm. Each image pair corresponds to the same swine scanned on different days. All images are shown at the same magnification and were obtained with a window width of 400 HU and a window level of 40 HU.

needed to optimize evaluation of specific disease states. Finally, although outer adipose-equivalent encasement diameters simulated overweight and obese adults, the anatomy of interest in the encased swine resembled that in small- to medium-size adults. The increased separation of abdominal organs by visceral fat that occurs in overweight patients was therefore not accurately modeled. However, the combination of solid plastic adipose-equivalent encasements and interstitial oil bags allowed for scan-to-scan conformity in overall abdomen shape and size, which is not otherwise possible. Although human studies are currently not possible due to lack of Food and Drug Administration approval, our findings provide data to justify future human studies.

In conclusion, an experimental tantalum oxide nanoparticle–based contrast agent provided improved vascular enhancement compared with a conventional iodinated contrast agent in swine models intended to simulate overweight and obese patients; this enhancement was measured by using both qualitative and quantitative metrics, including a comprehensive subjective reader grading study.

Author contributions: Guarantors of integrity of entire study, J.W.L., Y.S., B.M.Y.; study concepts/study design or data acquisition or data analysis/interpretation, all authors; manuscript drafting or manuscript revision for important intellectual content, all authors; approval of final version of submitted manuscript, all authors; agrees to ensure any questions related to the work are appropriately resolved, all authors; literature research, J.W.L., Y.S., Z.L., R.K., S.W., P.F.F., P.J.B., R.E.C., M.M., B.M.Y.; experimental studies, J.W.L., Y.S., C.S., Z.L., R.K., S.W., P.F.F., P.J.B., R.E.C., J.C.R., M.M., B.M.Y.; statistical analysis, J.W.L., Y.S., S.W.; and manuscript editing, J.W.L., Y.S., Z.L., R.K., S.W., P.F.F., P.J.B., J.C.R., P.M.E., M.M., B.M.Y.

Disclosures of Conflicts of Interest: **J.W.L.** disclosed no relevant relationships. **Y.S.** disclosed no relevant relationships. **C.S.** disclosed no relevant relationships. **Z.L.** disclosed no relevant relationships. **R.K.** disclosed no relevant relationships. **S.W.** disclosed no relevant relationships. **P.F.F.** Activities related to the present article: disclosed no relevant relationships. Activities not related to the present article: is a GE Global Research employee; holds employee shares in GE Global Research mutual funds; received a bonus from GE Global Research for filing a patent application related to this work. Other relationships: disclosed no relevant relationships. **P.J.B.** Activities related to the present article: disclosed no relevant relationships. Activities not related to the present article: was a General Electric and GE Global Research employee during data collection, the grant period, and manuscript writing and review. Other relationships: disclosed no relevant relationships. **R.E.C.** Activities related to the present article: disclosed no relevant relationships. Activities not related to the present article: is a GE Global Research employee; GE Global Research matches some 401k contributions; received a bonus from GE Global Research for filing a patent application related to this work. Other relationships: disclosed no relevant relationships. **J.C.R.** Activities related to the present article: disclosed no relevant relationships. Activities not related to the present article: is a GE Global Research employee. Other relationships: disclosed no relevant relationships. **P.M.E.** Activities related to the present article: disclosed no relevant relationships. Activities not related to the present article: is a GE Global Research employee; received a bonus from GE Global Research for filing a patent application related to this work. Other relationships: disclosed no relevant relationships. **M.M.** Activities related to the present article: disclosed no relevant relationships. Activities not related to the present article: was a General Electric employee during the study period. Other relationships: disclosed no relevant relationships. **B.M.Y.** Activities related to the present article: disclosed no relevant relationships. Activities not related to the present article: is a Nextrast board member; is a consultant for GE Healthcare; received grants from GE Healthcare, Philips Healthcare, and Guerbet; served as a speaker for GE Healthcare; received royalties from patents on CT contrast agents; holds stock in Nextrast; has been reimbursed for travel taken on behalf of Nextrast; is the co-inventor of a patent filed that came from work relevant to this study. Other relationships: disclosed no relevant relationships.

References

1. Yeh BM, FitzGerald PF, Edic PM, et al. Opportunities for new CT contrast agents to maximize the diagnostic potential of emerging spectral CT technologies. Adv Drug Deliv Rev 2017;113:201–222.
2. FitzGerald PF, Colborn RE, Edic PM, et al. CT image contrast of high-z elements: phantom imaging studies and clinical implications. Radiology 2016;278(3):723–733.
3. Carucci LR. Imaging obese patients: problems and solutions. Abdom Imaging 2013;38(4):630–646.
4. Kalender WA, Deak P, Kellermeier M, van Straten M, Vollmar SV. Application- and patient size-dependent optimization of x-ray spectra for CT. Med Phys 2009;36(3):993–1007.
5. Yu L, Li H, Fletcher JG, McCollough CH. Automatic selection of tube potential for radiation dose reduction in CT: a general strategy. Med Phys 2010;37(1):234–243.
6. Schindera ST, Tock I, Marin D, et al. Effect of beam hardening on arterial enhancement in thoracoabdominal CT angiography with increasing patient size: an in vitro and in vivo study. Radiology 2010;256(2):528–535.
7. Hainfeld JF, Slatkin DN, Focella TM, Smilowitz HM. Gold nanoparticles: a new x-ray contrast agent. Br J Radiol 2006;79(939):248–253.
8. Liu Y, Ai K, Liu J, Yuan Q, He Y, Lu L. A high-performance ytterbium-based nanoparticulate contrast agent for in vivo x-ray computed tomography imaging. Angew Chem Int Ed Engl 2012;51(6):1437–1442.
9. Roessler AC, Hupfer M, Kolditz D, Jost G, Pietsch H, Kalender WA. High atomic number contrast media offer potential for radiation dose reduction in contrast-enhanced computed tomography. Invest Radiol 2016;51(4):249–254.
10. Rabin O, Manuel Perez J, Grimm J, Wojtkiewicz G, Weissleder R. An x-ray computed tomography imaging agent based on long-circulating bismuth sulphide nanoparticles. Nat Mater 2006;5(2):118–122.
11. Jakhmola A, Anton N, Anton H, et al. Poly-ε-caprolactone tungsten oxide nanoparticles as a contrast agent for x-ray computed tomography. Biomaterials 2014;35(9):2981–2986.
12. FitzGerald PF, Butts MD, Roberts JC, et al. A proposed computed tomography contrast agent using carboxybetaine zwitterionic tantalum oxide nanoparticles: imaging, biological, and physicochemical performance. Invest Radiol 2016;51(12):786–796.
13. Nowak T, Hupfer M, Brauweiler R, Eisa F, Kalender WA. Potential of high-z contrast agents in clinical contrast-enhanced computed tomography. Med Phys 2011;38(12):6469–6482.
14. Torres AS, Bonitatibus PJ Jr, Colborn RE, et al. Biological performance of a size-fractionated core-shell tantalum oxide nanoparticle x-ray contrast agent. Invest Radiol 2012;47(10):578–587.
15. Lee N, Choi SH, Hyeon T. Nano-sized CT contrast agents. Adv Mater 2013;25(19):2641–2660.
16. Lambert JW, Edic PM, FitzGerald PF, Torres AS, Yeh BM. Complementary contrast media for metal artifact reduction in dual-energy computed tomography. J Med Imaging (Bellingham) 2015;2(3):033503.
17. Mongan J, Rathnayake S, Fu Y, et al. In vivo differentiation of complementary contrast media at dual-energy CT. Radiology 2012;265(1):267–272.
18. Rathnayake S, Mongan J, Torres AS, et al. In vivo comparison of tantalum, tungsten, and bismuth enteric contrast agents to complement intravenous iodine for double-contrast dual-energy CT of the bowel. Contrast Media Mol Imaging 2016;11(4):254–261.
19. Lambert JW, Sun Y, Gould RG, Ohliger MA, Li Z, Yeh BM. An image-domain contrast material extraction method for dual-energy computed tomography. Invest Radiol 2017;52(4):245–254.
20. Bonitatibus PJ Jr, Torres AS, Kandapallil B, et al. Preclinical assessment of a zwitterionic tantalum oxide nanoparticle x-ray contrast agent. ACS Nano 2012;6(8):6650–6658.
21. Frenzel T, Bauser M, Berger M, et al. Characterization of a novel hafnium-based x-ray contrast agent. Invest Radiol 2016;51(12):776–785.
22. Bae KT, Heiken JP, Brink JA. Aortic and hepatic peak enhancement at CT: effect of contrast medium injection rate—pharmacokinetic analysis and experimental porcine model. Radiology 1998;206(2):455–464.
23. Landis JR, Koch GG. The measurement of observer agreement for categorical data. Biometrics 1977;33(1):159–174.
24. Ha HI, Hong SS, Kim M-J, Lee K. 100 kVp low-tube voltage abdominal CT in adults: radiation dose reduction and image quality comparison of 120 kVp abdominal CT. J Korean Soc Radiol 2016;75(4):285–295.
25. Zaehringer C, Euler A, Karwacki GM, et al. Manual adjustment of tube voltage from 120 to 100 kVp during abdominal CT in patients with body weights ≤75 kg: assessment of image quality and radiation dose in a prospective, randomised trial. Clin Radiol 2016;71(6):615.e1–615.e6.
26. Baker ME, Karim W, Bullen JA, Primak AN, Dong FF, Herts BR. Estimated patient dose indexes in adult and pediatric MDCT: comparison of automatic tube voltage selection with fixed tube current, fixed tube voltage, and weight-based protocols. AJR Am J Roentgenol 2015;205(3):592–598.
27. Iannaccone R, Laghi A, Catalano C, et al. Hepatocellular carcinoma: role of unenhanced and delayed phase multi-detector row helical CT in patients with cirrhosis. Radiology 2005;234(2):460–467.
28. Kim SH, Kamaya A, Willmann JK. CT perfusion of the liver: principles and applications in oncology. Radiology 2014;272(2):322–344.
29. Ford ES, Maynard LM, Li C. Trends in mean waist circumference and abdominal obesity among US adults, 1999-2012. JAMA 2014;312(11):1151–1153.
30. Fitzgerald P, Lambert J, Edic P, et al. CT radiation dose at equal image contrast-to-noise ratio using iodine- and novel tantalum-based contrast agents: a large habitus phantom study [abstr]. In: Radiological Society of North America scientific assembly and annual meeting program. Oak Brook, Ill: Radiological Society of North America, 2015; 345.